High-resolution methods for fluorescence retrieval from space

Marina Mazzoni,[1,*] Pierluigi Falorni,[1] and Wouter Verhoef,[2]

[1]*Istituto di Fisica Applicata "Nello Carrara" del Consiglio Nazionale delle Ricerche, via Madonna del Piano 10, 50019 Sesto Fiorentino, Italy*

[2]*University of Twente, Faculty of Geo-Information Science and Earth Observation (ITC), Hengelosestraat 99, P.O. Box 6, 7500 AA Enschede, The Netherlands*

**M.Mazzoni@ifac.cnr.it*

Abstract: The retrieval from space of a very weak fluorescence signal was studied in the O_2A and O_2B oxygen atmospheric absorption bands. The accuracy of the method was tested for the retrieval of the chlorophyll fluorescence and reflectance terms contributing to the sensor signal. The radiance at the top of the atmosphere was simulated by means of a commercial radiative-transfer program at a high resolution (0.1 cm^{-1}). A test data set was generated in order to simulate sun-induced chlorophyll fluorescence at the top of the canopy. Reflectance terms were spectrally modeled using cubic splines and fluorescence by means of the sum of two Voigt functions. Sensor radiance residual minimization was performed in the presence of a multiplicative noise, thus ensuring that the sensor simulations were realistic. The study, which focused on the possibility of retrieving fluorescence with an accuracy better than 10%, was performed for instrument resolutions ranging from about 0.4 cm^{-1} to 2 cm^{-1} in order to test the algorithm for the characteristics of existing and planned hyper-spectral sensors. The algorithm was also used to retrieve fluorescence in the single O_2A band at the OCO and TANSO-FTS instrument spectral resolutions.

OCIS codes: (300.1030) Absorption; (300.6280) Spectroscopy, fluorescence and luminescence; (120.0280) Remote sensing and sensors; (280.4991) Passive remote sensing; (100.3190) Inverse problems.

References and links

1. K. Smorenburg, G. B. Courreges-Lacoste, M. Berger, A. Court, U. del Bello, G. Langsdorf, H. Lichtentha-ler, C. Sioris, M. P. Stoll, and H. Visser, "Remote sensing of solar-induced fluorescence of vegetation," Proc. SPIE **4542**, 178–190 (2002).
2. C. Buschmann, "Variability and application of the chlorophyll fluorescence emission ratio red/far-red of leaves," Photosynth. Res. **92**(2), 261–271 (2007).
3. N. Subash, and C. N. Mohanan, "Curve-fit Analysis of Chlorophyll Fluorescence Spectra: Application to Nutrient Stress Detection in Sunflower," Remote Sens. Environ. **60**(3), 347–356 (1997).
4. A. Kuze, H. Suto, M. Nakajima, and T. Hamazaki, "Thermal and near infrared sensor for carbon observation Fourier-transform spectrometer on the Greenhouse Gases Observing Satellite for greenhouse gases monitoring," Appl. Opt. **48**(35), 6716–6733 (2009).
5. H. Suto, A. Kuze, M. Nakajima, T. Hamazaki, T. Yokota, and G. Inoue, "Airborne SWIR FTS for GOSAT validation and calibration," Proc. SPIE **7106**, 71060M (2008).
6. R. Haring, R. Pollock, B. M. Sutin, and D. Crisp, "The Orbiting Carbon Observatory instrument optical design," Proc. SPIE **5523**, 51–62 (2004).
7. M. Meroni, and R. Colombo, "Leaf level detection of solar induced chlorophyll fluorescence by means of a subnanometer resolution spectroradiometer," Remote Sens. Environ. **103**(4), 438–448 (2006).
8. J. R. Miller, M. Berger, Y. Goulas, S. Jacquemoud, J. Louis, N. Moise, G. Mohammed, J. Moreno, I. Moya, R. Pedrós, W. Verhoef, and P. J. Zarco-Tejada, "Development of a Vegetation Fluorescence Canopy Model," ESTEC Contract No. 16365/02/NL/FF, Final Report, (2005).
9. S. Jacquemoud, and F. Baret, "PROSPECT: a model of leaf optical properties spectra," Remote Sens. Environ. **34**(2), 75–91 (1990).
10. W. Verhoef, and H. Bach, "Coupled soil-leaf canopy and amosphere radiative transfer modelling to simulate hyperspectral multi-angular surface reflectance and TOA radiance data," Remote Sens. Environ. **109**(2), 166–182 (2007).

#123414 - $15.00 USD Received 28 Jan 2010; revised 24 Feb 2010; accepted 2 Mar 2010; published 8 Jul 2010

11. M. Meroni, M. Rossini, L. Guanter, L. Alonso, U. Rascher, R. Colombo, and J. Moreno, "Remote sensing of solar induced chlorophyll fluorescence: Review of methods and applications," Remote Sens. Environ. **113**(10), 2037–2051 (2009).
12. M. Mazzoni, P. Falorni, and S. Del Bianco, "Sun-induced leaf fluorescence retrieval in the O_2-B atmospheric absorption band," Opt. Express **16**(10), 7014–7022 (2008).
13. S. Jacquemoud, F. Baret, B. Andrieu, F. M. Danson, and K. Jaggard, "Extraction of Vegetation Biophysical Parameters by Inversion of the PROSPECT+SAIL Models on Sugar Beet Canopy Reflectance Data. Application to TM and AVIRIS Sensors," Remote Sens. Environ. **52**(3), 163–172 (1995).

1. Introduction

Vegetation chlorophyll fluorescence is a small emission that may be less than 1% of the sensor signal at the top of the atmosphere (TOA). Its retrieval from space has been considered possible in certain absorption lines (Fraunhofer lines) in which solar radiation is strongly attenuated [1]. On-ground radiance measurements have been performed more frequently in other absorption lines, i.e., those belonging to the atmospheric O_2A oxygen band, due to their strategic position with respect to the FAR-RED chlorophyll emission bands. The other oxygen absorption band is also strategic, because of the proximity of the O_2B band to the chlorophyll RED emission band. In this work, we have focused our attention on the possibility of an accurate retrieval of chlorophyll fluorescence from space in both the O_2A (A for short) and O_2B (B for short) bands at the same time, in order to deduce as much as possible about plant functioning.

To obtain an accurate retrieval of any sort of information in these deeply-and narrowly-modulated absorption lines, high spectral resolution methods were necessary in both the forward modeling of radiation and fitting. The 10% level of accuracy in fluorescence was chosen as being useful for establishing correlations with photosynthetic activity [2], which represents a challenging goal for the limited spectral width of each observation window (about 20 nm each) as compared with the extension and shape of the chlorophyll fluorescence spectrum itself. On the ground, the fitting of an actively-induced full fluorescence spectrum at low resolution has been successfully explored [3] by means of spectroscopic functions. The fitting of passively-induced fluorescence in two limited and separate spectral ranges of the fluorescence spectrum necessarily involves dealing with some concomitant difficulties caused by the band separation, their small number and extension, and the radiation intensity modulation, all of which are non-existent in measurements performed with lasers. Furthermore, the advantage of using these atmospheric absorption bands from space is reduced, due to a re-absorption of the fluorescence itself and to the presence of other signals, such as those of the atmospheric scattering processes, which are absent on the ground, and contribute to the sensor signal at TOA.

Therefore, a new methodology was necessary, one that included the construction of a data set of variability ranges for the fitting parameters and a procedure for attaining of the required accuracy in retrieving the fluorescence notwithstanding the coupling that occurred between the functions used for fitting both the reflectance and the fluorescence. This construction was done in the presence of a multiplicative sensor noise which was added to the simulated sensor radiance for the purpose of arriving at reliable applications.

By way of a demonstration, we combined forward modeling at the maximum spectral resolution of 0.1 cm^{-1} of the MODTRAN5 program (beta version) with spectral fitting for a VIS-NIR interferometer/spectrometer resolutions of 0.38 cm^{-1} [4,5] and 0.77 cm^{-1} [6]. These represent the spectral resolutions of existing instruments for space observations in the O_2A atmospheric absorption band. Furthermore, we studied the retrieval for a resolution of 2 cm^{-1}, which was very close to that of a commercial instrument used on the ground for vegetation monitoring in the A and B bands [7] at relatively high resolution. The spectral resolutions and samplings were compared for the same spatial resolution of about 300m.

Since the observable fluorescence and reflectance of interest were at canopy level, we used a test data set generated by simulations performed by means of a program (FluorSAIL [8]) that comprised a leaf-canopy model for producing the vegetation signal at the top and bottom of the canopy for computed vertical flux profiles of solar irradiation. Moreover, both direct and diffuse reflectance factors were considered, together with adjacency effects that could

#123414 - $15.00 USD Received 28 Jan 2010; revised 24 Feb 2010; accepted 2 Mar 2010; published 8 Jul 2010

contribute to the sensor radiance. Two cases were treated which we named *same* and *bare* depending on the type of surroundings of the same or different soil type as the (vegetated) target, respectively. In this paper the comparative study at the three different resolutions and the analysis in the single A band at the OCO [6] and TANSO-FTS [4] instrument spectral resolutions was performed only for this case. Furthermore, the fluorescence retrieval in both bands was also performed at the TANSO-FTS spectral resolution by using the results obtained in the single A band: a two-step retrieval which greatly enhanced accuracy for high noise values.

2. Fluorescence and reflectance

To determine the adequacy of the mathematical models that we used in the retrieval, we used a test data set generated for canopy fluorescence and reflectance. Both simulations were based on a leaf fluorescence model, which in turn was based on a model of leaf optical properties [9] and on vertical profiles of the direct solar and diffuse upward and downward fluxes inside the canopy. The changes in their spectral profiles that were induced by the canopy interceptions of radiation were considered for both direct and diffuse radiation. The program FluorSAIL [8] computed these profiles by means of an analytic (canopy) radiative transfer sub-routine called 4SAIL [8,10]. In Fig. 1, we show a series of canopy fluorescence line-shapes which were obtained for different chlorophyll contents (Cab), a leaf area index (LAI) of 4 and a moderately erectophile leaf angle distribution.

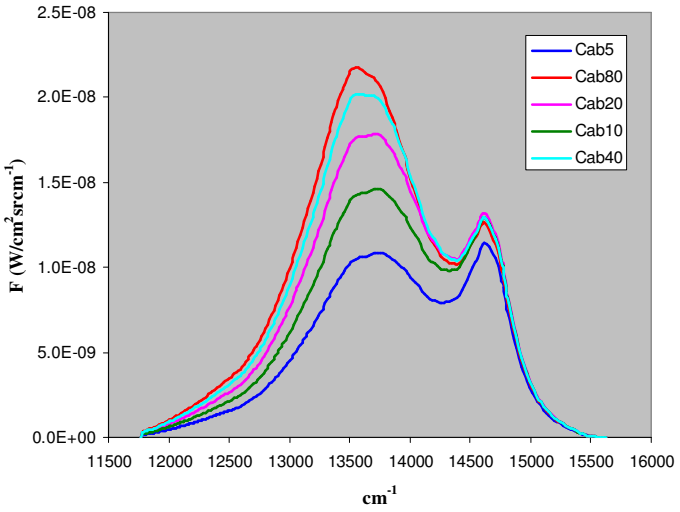

Fig. 1. Simulated canopy fluorescence for different Cab values

Bidirectional reflectance effects are characterized by four relevant reflectance terms were identified, two of which (i.e. r_{so} and r_{do}, the directional reflectance factors for solar and sky radiation) referred to the target, while the other two (i.e. $\overline{r_{sd}}$ and $\overline{r_{dd}}$) represented the hemispherical reflectance factors for solar and sky radiation of a larger area including also the surroundings of the target pixel. For the applied terminology, see also section 3. In the retrieval procedure, the reflectance was fitted - by means of cubic spline functions - with knots, the number of which depended on the reflectance variability as a function of wavenumber and the desired accuracy in fluorescence retrieval for the level of noise that was present. These and canopy fluorescence were deduced in the atmospheric conditions and observation angle which are reported in the third paragraph.

The fluorescence that we used for an evaluation of the accuracy in fluorescence retrieval at the different spectral resolutions is shown in Fig. 2. It was characterized by an Fmax intensity maximum that was in the A band equal to 1.24×10^{-8} W/cm^2 sr cm^{-1}, and by a ratio of the

#123414 - $15.00 USD Received 28 Jan 2010; revised 24 Feb 2010; accepted 2 Mar 2010; published 8 Jul 2010

peaks of the A and B bands that was equal to 1.13. Sensor radiance at TOA (as obtained at a resolution of 0.38 cm^{-1} from Eq. (6) was also shown in order to point out the position of the two (i.e. A and B) windows.

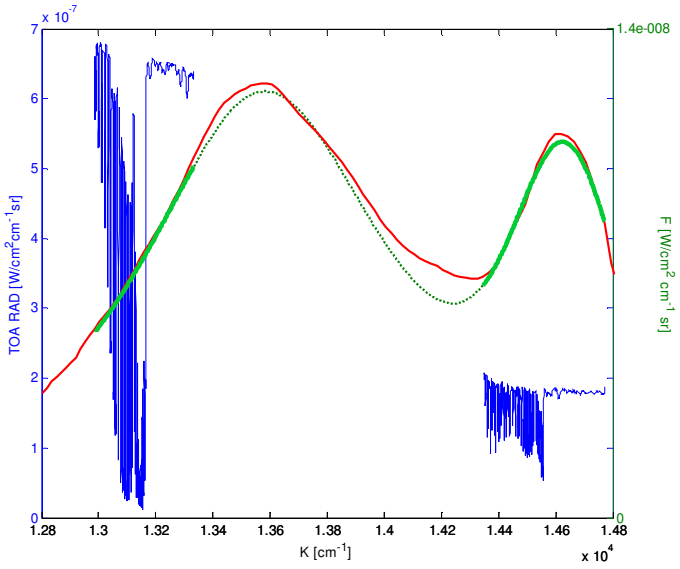

Fig. 2. Simulated canopy fluorescence (red line) with retrieved fluorescence in the A and B bands (heavy green line) shown also outside (as a dotted line). Fluorescence was retrieved in the *(A-AB)* case reported in Table 4 for a resolution equal to 0.38 cm^{-1}. Sensor radiance at TOA (blue line) in the A and B bands is also shown for the same *ILS*.

A faithful reproduction of fluorescence in the two spectral windows is required in order to monitor the state of health of plants during their diurnal and seasonal evolution. As reported by Meroni et al. in [11], spectral fitting and the retrieval of both fluorescence and reflectance was considered to be a promising method for reaching this goal. On the ground, spectral fitting has already been demonstrated to be feasible at the resolution of 2 cm^{-1} [7,11] and 0.5 cm^{-1} [12,11]. However, up until now, it has been performed only in separate parts of the fluorescence spectrum and with different polynomials for fluorescence fitting in the two bands. In the present work, the fitting of the FluorSAIL simulated fluorescence was performed by means of the sum of two Voigt functions (8 parameters) in both the A and B bands. This choice was found to be more adequate with respect to the sum of two Gaussians, which were also tested and to which the Voigt could reduce when the minimization algorithm so required. In fact, more than two Voigt or Gaussian functions were required in order to simulate the full fluorescence spectrum. However, in this case of spectral fitting in separate and quite distant spectral windows, we could reduce the number of Voigts to two since the reciprocal influence of these distant lines could be simulated by means of their non-constant and Lorentzian contribution in the wings. Further information such as the ratio ρ between the peaks of the two major emission bands would be desirable. Since the FAR-RED peak is positioned outside the corresponding observation window, the accuracy in the fluorescence retrieval within this window is merely a prerequisite for obtaining this goal which only an appropriate choice of the spectroscopic function employed for fitting fluorescence could make possible. In Fig. 2, the dotted line is the function marked in green that was retrieved in the two A and B bands. Indeed, we verified that the ratio ξ of the two peaks of the function used to fit fluorescence was very close (better than 10%) to ρ when the fluorescence accuracy was within 10% despite the asymmetry of the fluorescence line-shape and the fact that the peak position of the Voigt function at the O_2A band (Voigt A) could be slightly different from that of the FAR-RED fluorescence peak as shown in Fig. 2.: ξ might thus be considered a useful parameter for data

#123414 - $15.00 USD Received 28 Jan 2010; revised 24 Feb 2010; accepted 2 Mar 2010; published 8 Jul 2010

assimilation in the future. The requirements regarding fluorescence retrieval were assigned in terms of the Relative Root Mean Square Error % (RRMSE%) as compared with the magnitude of the value observed.

3. Sensor radiance

In this section we introduce the forward model for calculating the radiance at TOA, which was inferred from the coupled atmospheric-canopy model reported in [10] for a non-Lambertian target and surroundings. The TOA spectral radiance including a solar-induced fluorescent radiance contribution F_s at BOA (bottom of the atmosphere) level can be described by the equation:

$$L_o^{\mathrm{TOA}} = L_0 + F_s\tau_{oo} + E_s^o \frac{\cos\theta_s}{\pi}\left[\left(\tau_{ss}r_{so} + \frac{\tau_{sd} + \tau_{ss}\overline{r_{sd}}\rho_{dd}}{1-\overline{r_{dd}}\rho_{dd}}\, r_{do}\right)\tau_{oo} + \frac{\tau_{ss}\overline{r_{sd}} + \tau_{sd}\overline{r_{dd}}}{1-\overline{r_{dd}}\rho_{dd}}\,\tau_{do}\right] \quad (1)$$

For the terminology of the quantities other than F_s and the surface reflectances, already introduced in section 2, reference is made to [10] where Eq. (1) was published without the fluorescence contribution. The term L_0 is the atmospheric path radiance for a black earth surface, and E_s^o is the extra-terrestrial solar irradiance on a plane perpendicular to the sunrays. The solar zenith angle is given by θ_s, and the double-subscripted ρ and τ terms indicate respectively reflectances and transmittances of the whole atmosphere for direct and diffuse incident and scattered radiation types, where the first subscript refers to the incident radiation (*s* for direct solar radiation, *d* for diffuse sky radiation, and the second subscript to the scattered radiation (*o* for direct radiation in the observer's direction, *d* for hemispherical diffuse radiation). The same subscripts are used for the *r* terms, which characterise surface reflectance. The successive terms on the right-hand side of Eq. (1) can be attributed to:

1)Atmospheric path radiance, 2) Target fluorescence (radiance), 3) Bidirectional reflectance for solar irradiance, 4) Directional reflectance of sky irradiance (2 contributions), 5)Adjacency effect (2 contributions).

The adjacency effect depends on the spatially filtered reflectance quantities $\overline{r_{sd}}$ and $\overline{r_{dd}}$, which are hemispherical reflectances for direct solar and diffuse incident sky radiation, respectively. For sensors with a moderate spatial resolution of ~300m, a significant contribution to the spatial filter actually comes from the target pixel, not from the surroundings of the pixel. For lower resolutions like that of TANSO-FTS (e.g. 10 km), the whole adjacency effect is included in the pixel. From a Monte Carlo simulation, this contribution was estimated to be 45% for a normal visibility of 23 km. This means that in this case the spatially filtered reflectances should be estimated by:

$$\begin{aligned}\overline{r_{sd}} &= 0.45 r_{sd}(\text{target}) + 0.55 r_{sd}(\text{surr.})\\ \overline{r_{dd}} &= 0.45 r_{dd}(\text{target}) + 0.55 r_{dd}(\text{surr.})\end{aligned} \quad (2)$$

Strictly, the given TOA radiance equation is only valid for infinitely narrow spectral bands or for spectral intervals in which all variables can be considered spectrally constant. Otherwise, curve-of-growth effects can occur, and a careful spectral resampling of products of spectral variables is required. Curve-of-growth effects in general refer to the phenomenon that the atmospheric transmittance of absorption lines does not follow Beer's Law when there are large variations of the spectral absorption within the interval. Spectral resampling is denoted by placing quantities within < > brackets. This gives an equation which is also valid for wider spectral intervals and therefore can be applied in more practical situations:

#123414 - $15.00 USD Received 28 Jan 2010; revised 24 Feb 2010; accepted 2 Mar 2010; published 8 Jul 2010

$$
\begin{aligned}
< L_o^{\mathrm{TOA}} > = & < L_0 > + < \tau_{oo} > F_s \\
& + \frac{\cos\theta_s}{\pi}\left(< E_s^o \tau_{ss} \tau_{oo} > r_{so} + \frac{< E_s^o \tau_{sd} \tau_{oo} > + < E_s^o \tau_{ss} \tau_{oo} \rho_{dd} > \overline{r_{sd}}}{1 - \overline{r_{dd}} < \rho_{dd} >} r_{do} \right) \\
& + \frac{\cos\theta_s}{\pi}\left(\frac{< E_s^o \tau_{ss} \tau_{do} > \overline{r_{sd}} + < E_s^o \tau_{sd} \tau_{do} > \overline{r_{dd}}}{1 - \overline{r_{dd}} < \rho_{dd} >} \right)
\end{aligned}
\tag{3}
$$

Here, it was tacitly assumed that fluorescence and the reflectances can be considered constant over the spectral interval, which however for resolutions better than about 10 cm^{-1} is a fair approximation. In the above expression one may identify the following spectrally resampled terms:

$$
\begin{aligned}
t_1 &= < L_0 > \\
t_2 &= < \tau_{oo} > \\
t_3 &= < \rho_{dd} > \\
t_4 &= < E_s^o \tau_{ss} \tau_{oo} > \cos\theta_s / \pi \\
t_5 &= < E_s^o \tau_{sd} \tau_{oo} > \cos\theta_s / \pi \\
t_6 &= < E_s^o \tau_{ss} \tau_{oo} \rho_{dd} > \cos\theta_s / \pi \\
t_7 &= < E_s^o \tau_{ss} \tau_{do} > \cos\theta_s / \pi \\
t_8 &= < E_s^o \tau_{sd} \tau_{do} > \cos\theta_s / \pi
\end{aligned}
\tag{4}
$$

The TOA radiance equation can now be written as:

$$
L_o^{\mathrm{TOA}} = t_1 + t_2 F + t_4 r_{so} + \frac{t_5 + t_6 \overline{r_{sd}}}{(1 - t_3 \overline{r_{dd}})} r_{do} + \frac{t_7 \overline{r_{sd}} + t_8 \overline{r_{dd}}}{1 - t_3 \overline{r_{dd}}}
\tag{5}
$$

This result shows that the TOA radiance signal is a function of the atmospheric path radiance, the TOC fluorescent radiance, two canopy reflectances summarising the BRDF effects, two effective hemispherical reflectances of the surroundings, and eight spectrally variable atmospheric 'constants'. This radiance expression was used to evaluate the source of uncertainties that resulted from adjacency effects and scattering terms of different origin.

In Eq. (5), t_1 is the atmospheric (black earth) path radiance, t_2 is the target-sensor transmittance, t_3 is the spherical albedo of the bottom of the atmosphere, and the subsequent t_i terms (i = 4, 5, 6, 7, 8) are radiance terms (in the same units as t_1 and F) that determine the various surface-reflectance contributions. The t_1-t_8 terms were extracted by using a MODTRAN Interrogation Technique (MIT) [10] which is based on a series of 4 runs that covered both the O_2 absorption bands (i.e. 677nm – 697nm and 750nm – 770nm) with a nadir viewing sensor situated at 800 km above a ground altitude of 200m. The sun was at a zenith angle of 30°, and the visibility was 23 km. A rural aerosol type and a mid-latitude summer atmosphere were selected. Outputs were obtained for the maximum MODTRAN5 resolution, i.e. 0.1 cm^{-1}, and comprised about 7700 data points. In reality, the TOA radiance spectrum is influenced by clouds, cloud shadows and spatially variable amounts of aerosol. Areas of clouds and cloud shadows should be detected and flagged as unsuitable for further processing. Spatially variable haze can be a serious problem, as this might be mistaken for spatial fluorescence variations. However, a fluorescence sensor will not operate in isolation, and it is expected that spatial haze variations can be retrieved from complementary multi-or hyperspectral observations from a broader spectral (VIS-NIR) range. It might be possible to detect haze variations in the O_2A and O_2B regions, and also aerosol variations, but this would need more investigations.

For the retrieval, we adopted the scheme of using only two functions, one for each couple of reflectances according to their origin, and to retrieve fluorescence by evaluating two

#123414 - $15.00 USD Received 28 Jan 2010; revised 24 Feb 2010; accepted 2 Mar 2010; published 8 Jul 2010

"more-synthetic" [13] reflectances at the same time. They were called RSDO and RSDD for target and surroundings, respectively and were retrieved imposing RSDO = r_{so} = r_{do} and RSDD = r_{sd} = r_{dd}. A proxy of the Lambertian case was obtained by forcing the algorithm to the retrieval of a single reflectance term RS for all the r_{ij} terms in Eq. (5).

The sensor radiance (*SENSOR_RAD*) at TOA was obtained from the convolution of the total radiance with the Instrumental Line Shape (*ILS*) of the detection instrument as:

$$SENSOR\_RAD = [L_o^{\mathrm{TOA}}] \otimes ILS \tag{6}$$

where ⊗ indicates the convolution operation. In the absence of measurements, *F* and r_i (i = *so, do, sd, dd*) were the simulated output files and *ILS* is a Gaussian function. For the retrieval, a function: *SENSOR_RADm*, was generated by inserting in (6) the mathematical functions F_m, r_m, and ILS_m which represented the unknowns in place of the simulated values. To simulate the convolution operation correctly using the instrument *ILS*, the maximum resolution outputs of MODTRAN5 were found to be sufficient for satisfying the Nyquist criterion in the sampling of the signals. Particular attention was paid to building the Voigt profiles used in this work for modeling *ILS* and simulated fluorescence. Both functions were defined in the Fourier-transform domain in order to avoid aliasing and distortions in the retrieved signals. After re-sampling the signals from the MODTRAN5 minimum sampling (0.1 cm^{-1}) to that of the instrument, Eq. (6) was reduced to a set of *l* equations, one for each sampled value of the sensor radiance to which Gaussian noise was added in order to produce *SENSOR_RADn*. In order to represent the influence of a photon-noise limited sensor, the noise was characterized by means of a standard deviation proportional by a factor *n* to the square root of the signal. The signal-to-noise ratio SNR reported in the paper figures was computed according to the following equation where the root mean square (rms) of the difference between noisy and non-noisy sensor signal is employed for an evaluation of noise:

$$SNR = SENSOR\_RAD / rms\left(SENSOR\_RAD - SENSOR\_RADn\right) \tag{7}$$

The direct problem was defined by equating the functions N*SENSOR_RADn* with N*SENSOR_RADm* which were obtained by dividing each equation by its corresponding *SENSOR_RAD* value or by the square root of *SENSOR_RAD* to weigh the signal uniformly in both the A and B bands or to make the statistical component independent on wavenumber, respectively. The minimization procedure was performed on the difference *DS*:

$$\mathrm{DS} = \mathrm{NSENSOR\_R\ ADn} - NSENSOR\_RADm \tag{8}$$

between the normalized functions, and produced the residuals which are reported in the figures as being multiplied by 100 with the name PRG. In the same figures, the values obtained by dividing all the equations by *SENSOR_RADmax*, the maximum of *SENSOR_RAD* in the two fitting windows, were also shown with the name TRU for purposes of comparison. The LSQCURVEFIT was the Least Square Program of MATLAB7 that minimized the PRG residuals in order to find the set of parameter values for F_m, r_m, and ILS_m by means of a best-fit procedure. The retrieval algorithm and fitting process evaluated all the equations. The Relative Root Mean Square Error (*RRMSE%*), as compared with the magnitude of the observed fluorescence in conjunction with residuals, was used to evaluate the results of the fitting.

4. Parameter-set construction

One of the procedures employed successfully for attaining sensor radiance minimization and accurate fluorescence retrieval at the same time consists of the construction of a data set for the variability range of each parameter. This particular data set, which was constructed for an instrument resolution of 2 cm^{-1}, was controlled at the other two resolutions (e.g. 0.77 cm^{-1} and 0.38 cm^{-1}). Delimitation of the parameter variability range is a commonly used procedure for speeding up the convergence of the minimization algorithm, and is done *a priori*. In our case, the ranges were initially established as widely as possible, to allow the minimization

#123414 - $15.00 USD Received 28 Jan 2010; revised 24 Feb 2010; accepted 2 Mar 2010; published 8 Jul 2010

algorithm to work without constraints in a direct retrieval procedure that employed only part of them (*e.g*. the Voigt parameters) for known reflectance terms. We deduced the k_0 ratio between the Voigt intensities for zero noise from this first step. In the successive optimization phases, k_0 was found to be a useful parameter in establishing the noise limit value. The optimized variability ranges of the reflectance parameters, their number, and the optimized variability ranges of the fluorescence parameters were examined for increasing noise by retrieving fluorescence and reflectance terms in successive runs, each of which corresponded to a randomly-generated noise. The latter were deduced by means of successive restrictions on the variability ranges of reflectance and fluorescence parameters in the (two) A and B windows. Since there were many local minima, which were mainly due to the coupling between the retrieved reflectance terms and the fluorescence, it was possible that one of the two Voigts could prevail over the other, depending on the type of retrieved reflectance (single or double) or normalization (to SENSOR_ RAD or to its square root).

5. Retrieval

For an actual retrieval, we identified a set of parameters (i.e. the Voigt amplitudes and reflectance ranges) the variability ranges of which should necessarily be left wider at the beginning in order to enable a numerical estimate of the unknown fluorescence and reflectance terms. In particular, notwithstanding the fact that the fluorescence for Cab values higher than 5 was expected to be higher than 10^{-8} W/cm^2 sr cm^{-1}, the Voigt amplitudes were initially made to vary between 0 and 2 times the amplitude of the simulated fluorescence in order to cover all the possibilities.

Table 1. Fluorescence accuracy in the A and B bands for different noise coefficients

ILS cm^{-1}	*samp. cm^{-1}*	*RRMSE_FA*	*RRMSE_FB*	*n*
0.380	0.200	0.45	0.67	0
		0.41	0.70	10^{-6}
		0.78	0.83	2.4 10^{-6}
		2.04	1.07	4.2 10^{-6}
	0.317	0.44	0.67	0
		0.60	0.77	10^{-6}
		1.26	1.15	2.4 10^{-6}
		2.5	1.92	4.2 10^{-6}
7	3.68	1.66	0.68	0
		2.57	1.16	10^{-6}
		3.83	2.23	2.4 10^{-6}
		5.88	3.66	4.2 10^{-6}
	5.84	1.90	0.68	0
		3.40	2.35	10^{-6}
		6.33	4.69	2.4 10^{-6}
		10.68	7.96	4.2 10^{-6}

#123414 - $15.00 USD Received 28 Jan 2010; revised 24 Feb 2010; accepted 2 Mar 2010; published 8 Jul 2010

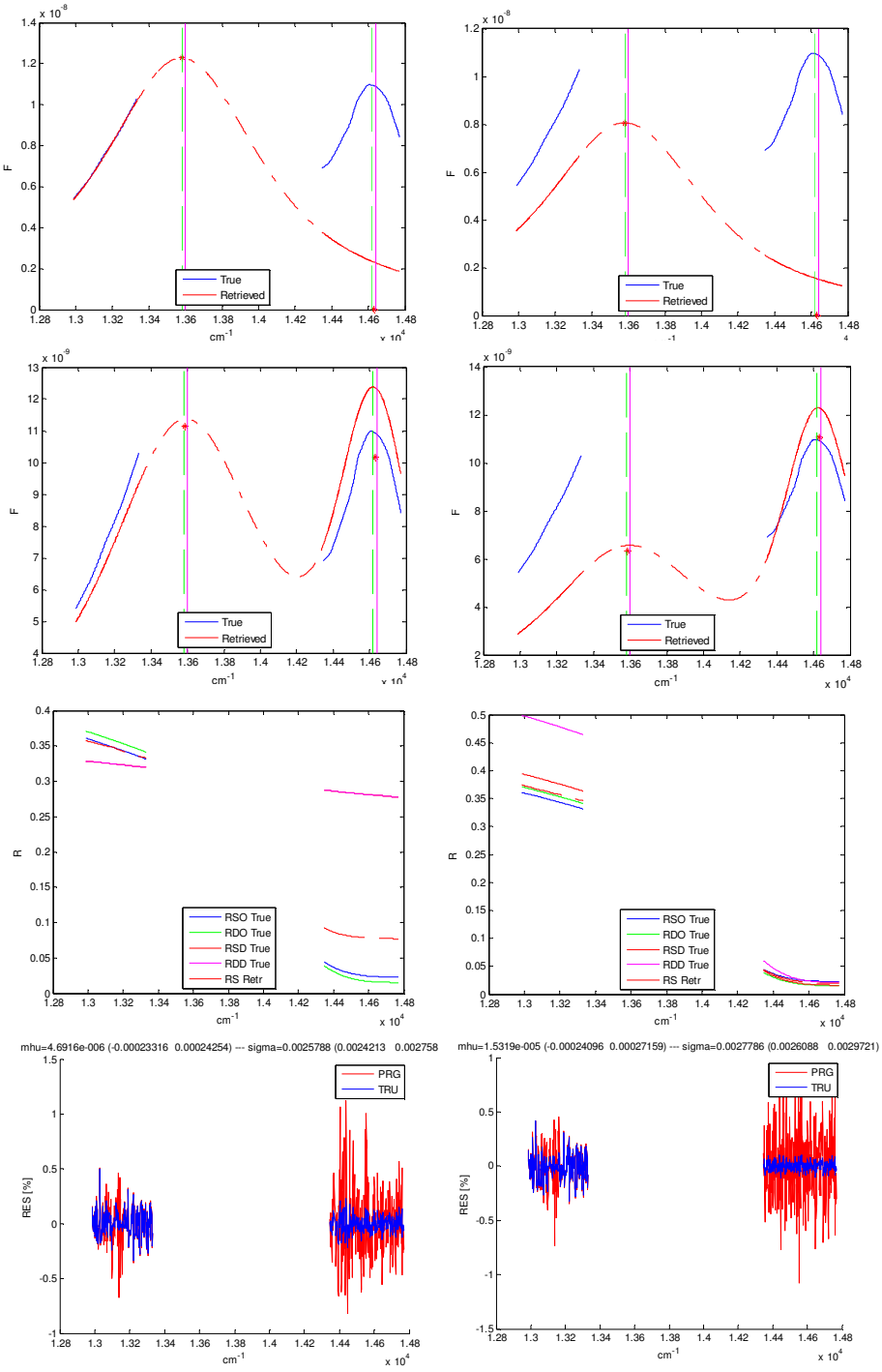

Fig. 3. The images in the first row refer to the fluorescence retrieved in the two A and B bands in both *bare* (left) and *same* (right) cases for n = 10^{-6} and a resolution of 2 cm^{-1}. A complete series of simulated and retrieved fluorescences (second row), simulated reflectances and retrieved RS term (third row), and residuals (fourth row) for a different randomly-generated noise of same n, for *bare* (first column) and *same* (second column) cases. *DS* were normalized to SENSOR-RAD. In the *bare* case, the difference between RS and r_{so} (RSO) in the B band is significant. The two simulated adjacency reflectance terms were equal. In the *same* case, RS was found closer to r_{do} (RDO) than to r_{so} (RSO), in the A band.

#123414 - $15.00 USD Received 28 Jan 2010; revised 24 Feb 2010; accepted 2 Mar 2010; published 8 Jul 2010

All the other parameters were left restricted and equal to the values found in the parameter-set construction, since they could thus cover many simulated line-shapes, even ones that were different from the one dealt with in this work, while granting an accurate retrieval also in the presence of a realistic noise.

Furthermore, the same generated noise was used in all the successive minimization runs for simulating real measurement conditions. In all the figures, the peak position and intensity of each Voigt are indicated by an asterisk and their variability range, by vertical lines.

To evaluate the role of spectral resolution for the function chosen to fit the fluorescence, we performed fluorescence retrieval for known reflectance terms for two extreme resolutions and four different samplings, with and without noise. The results are reported in Table. 1 in terms of the fluorescence *RRMSE_FA* and *RRMSE_FB* in the two A and B bands, respectively, and were obtained in a single run. The samplings, which were a fraction of the corresponding *ILS*, and were $(1.2)^{-1}$ and $(1.9)^{-1}$ times the respective resolutions.

The maximum noise in Table 1 corresponded to the limit value for a resolution of 7 cm^{-1}.

The high resolution results revealed the quality of the function used. At the lower resolution, the accuracy decreased. A smaller sampling revealed important for improving the accuracy in correspondence with a high noise value. However, it is difficult to imagine a retrieval that has the possibility of using reflectance parameters known with an "unlimited" accuracy, as in the example reported. We performed this exercise only to emphasize the differences in the results obtained at two very different resolutions. For fluorescence and reflectance terms retrievals, the paired reflectance terms according to their origin was found to be much more useful than the single-reflectance term. This is because the use of the latter could not provide a sufficiently accurate retrieval of fluorescence when the variability ranges were large. To demonstrate this fact, in Fig. 3 a complete series is shown for *bare* (first column) and *same* (second column) cases for Voigt amplitudes which could vary between 0 and 2 times the amplitude of the simulated fluorescence. The series is reported in the last three rows and consisted of simulated and retrieved fluorescences, simulated reflectances and retrieved RS term, and residuals for both the A and B bands. These were obtained for the same randomly-generated noise of coefficient $n = 10^{-6}$ and a resolution of 2 cm^{-1}. The peak position and intensity of each Voigt is indicated by an asterisk. The retrieval failed to achieve its goal because fluorescence accuracy was much lower than 10%, especially for the *bare* case. In Fig. 3, the images in first row refer to the fluorescence obtained for a different randomly-generated noise from the one used in the retrieval of the complete series. We have shown this in order to emphasize the effect on fluorescence of a realistic noise which may have a mean value that is different from zero. For the reflectance term retrieval, we used 12 knots in both windows (shortly {12,12}) in both cases. It is interesting to note the influence of the adjacency terms on RS in the A (*same* case) and B bands (*bare* case), respectively: it emphasizes the importance of adequately considering their effects in the retrieval of fluorescence.

The choice of the paired reflectance terms was more robust, since a better decoupling of the reflectance terms from the fluorescence was possible by successive optimizations. In particular, the oscillations in the retrieved reflectance terms could suggest the successive restrictions on the variability ranges of reflectance terms, especially when the minimization algorithm was working at in far from optimal conditions. The strategy of the retrieval procedure was the same one used for the parameter-set construction, and consisted of successive optimizations in which also the Voigt amplitude ranges were restricted in accordance with the results of the previous runs in order to make it possible to discover the local minimum that minimized fluorescence uncertainty and not only that of sensor radiance. Several runs were required in order to decouple the florescence from the reflectance terms. This number depended on the noise and the resolution. The procedure was halted when the reflectance characteristics stopped being useful in guiding successive steps and when the Voigt amplitudes changed less than about 2% under modified initial conditions, for all the resolutions.

#123414 - $15.00 USD Received 28 Jan 2010; revised 24 Feb 2010; accepted 2 Mar 2010; published 8 Jul 2010

For the *bare* case, the retrievals were obtained with initial variability ranges of both reflectance terms which were limited to between 0 and 0.4 and for Voigt amplitudes which could vary between 0 and 2 times the amplitude of the simulated fluorescence. The variability range of reflectance terms was about 10% greater than that of the simulated target function variation and about seven time larger than that of the simulated adjacency function variation. This width of the latter was left this way due to the scarce information on the adjacency term that can be derived from the retrieval performed in the Lambertian case (see Fig. 3, first image in the third row, for example) and to avoid overfitting, especially for high noise values.

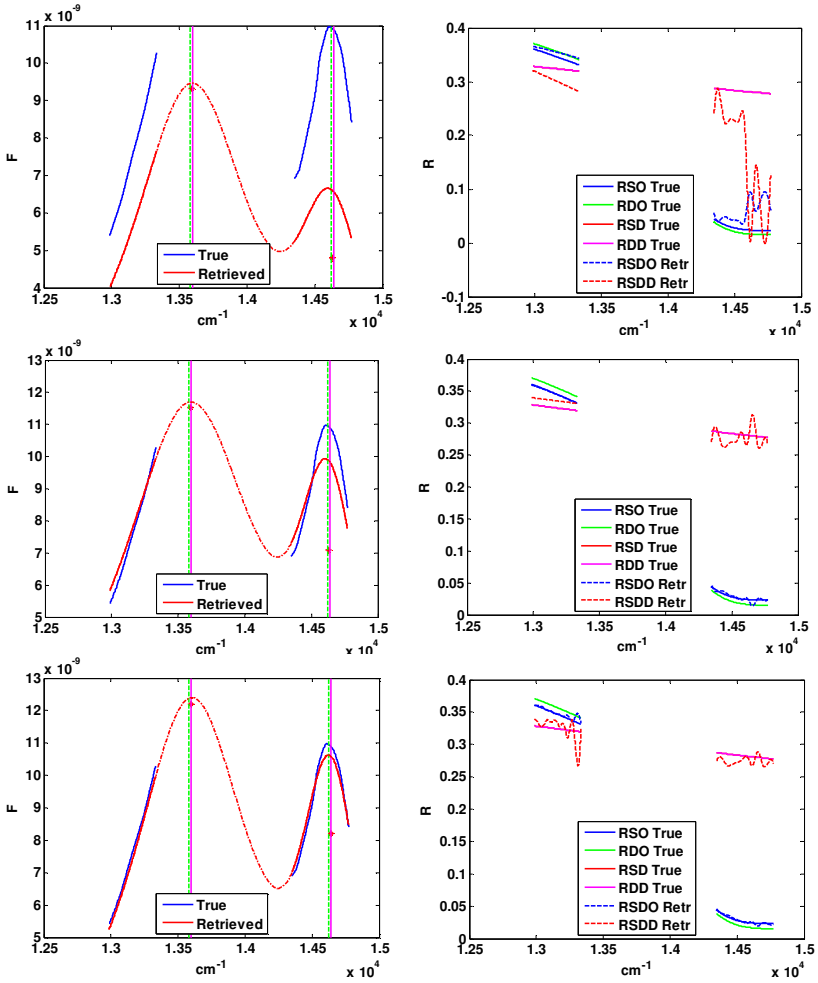

Fig. 4. Some of the fluorescences (left) and paired reflectance terms (right) results of a series of 8 runs obtained for *bare* case at a resolution of 2 cm^{-1} and noise coefficient $n = 10^{-6}$. DS derived from a normalization to SENSOR-RAD. The peak position and intensity of each Voigt are indicated by an asterisk. The two simulated adjacency reflectance terms were equal. The first row are the results of the first run for which reflectance terms variability range was set between 0 and 0.4 while the amplitude variability range of the two Voigts was set from 0 and 2 times the amplitude of the simulated fluorescence SFA. The second row are the results of the fourth run for which, according to the results of the third run, reflectance RSDO variability range was set between 0 and 0.36, reflectance RSDD variability range between 0.265 and 0.340 while the amplitude variability range of the Voigt A was set from 0.93 and 2 times SFA and that of Voigt B between 0.57 and 2 times SFA, respectively. The third row are the results of the last run and were obtained for an increased number of knots. According to the results of the previous runs, reflectance RSDO variability range was left between 0 and 0.36, the reflectance RSDD variability range was set between 0.268 and 0.340 while the amplitude variability range of the Voigt A was set between 0.98 and 2 times SFA and that of Voigt B between 0.65 and 2 times SFA, respectively.

#123414 - $15.00 USD Received 28 Jan 2010; revised 24 Feb 2010; accepted 2 Mar 2010; published 8 Jul 2010

The adjacency terms were found to be correlated to the target reflectance in both the B and A bands, and the corresponding parameters were limited for first in the successive runs. The dominant target reflectance term was r_{so}.

In Fig. 4, we report the results obtained with the randomly-generated noise (which was saved as a file in the procedure) and n coefficient that were used to obtain the complete series shown in Fig. 3. These results which were obtained with the two paired reflectances scheme are commented on briefly here as follows. In the first four runs, we used {3,12} knots for RSDO and {2,12} for RSDD. It was possible for the number of knots to be low only in the A band, due to the shape of the target reflectance. In the fourth run we obtained a fluorescence (first image in the second row of Fig. 4) *RRMSE%* of 4.24% and 7.66% in the A and B bands, respectively. The effects of an increased number of knots: {12,12} for both reflectance terms made it possible in the eighth run to obtain a less distorted fluorescence shape (first image in the third row of Fig. 4) and a fluorescence *RRMSE%* of 2.37% and 2.75% in the said A and B bands. We want to notice that the most relevant drop appear in the adjacency reflectance term, and that is sited in the A band, in correspondence of the continuum.

In the *same* case, and for the same noise n value, the *RRMSE%* values for fluorescence as compared with those of the *bare* case were slightly more favourable in the A band, and slightly less favourable in the B band, as could be expected considering the difficulty in decoupling proximal reflectance terms (see image in the second column, third row of Fig. 3). In the retrieval, reflectance fitting functions were initially limited to a range of about 10% and 20% wider than the adjacency and target reflectance term variations, respectively.

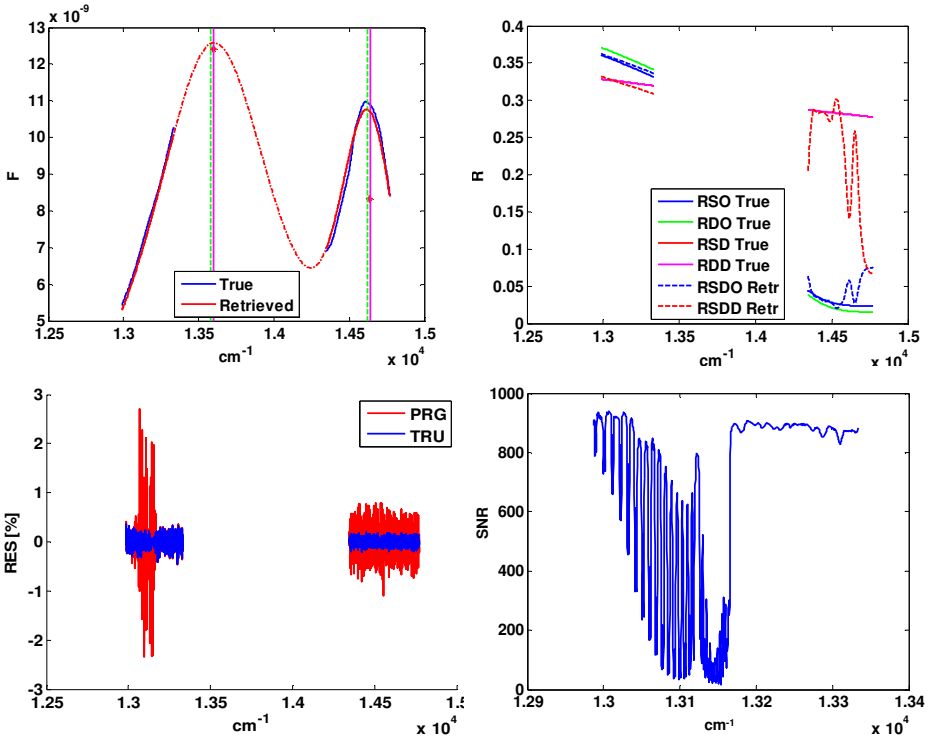

Fig. 5. Single-run retrieval of fluorescence, reflectance terms, and residuals for *bare* case at a resolution of 0.38 cm^{-1}, sampling 0.2 cm^{-1}, and noise coefficient $n = 10^{-6}$. The corresponding SNR is also reported. The peak position and intensity of each Voigt are indicated by an asterisk. DS derived from a normalization to SENSOR-RAD. The peak position and intensity of each Voigt is indicated by an asterisk. The two simulated adjacency reflectance terms were equal.

These limits, especially for the adjacency term in the A band, could be deduced by a run which was performed for the Lambertian case (similar to the one shown in Fig. 3), under the

#123414 - $15.00 USD Received 28 Jan 2010; revised 24 Feb 2010; accepted 2 Mar 2010; published 8 Jul 2010

assumption that, according to the sensor radiance simulations, the contribution deriving from the term $\overline{r_{dd}}$ (RDD in Fig. 3) had a much smaller influence than that of the term $\overline{r_{sd}}$ (RSD in Fig. 3), which in turn should be close to the target reflectance terms. At a resolution of 0.38 cm^{-1}, the number of runs could be reduced to only one, in order to obtain the same goal in correspondence with the same value of $n = 10^{-6}$. For the case reported in Fig. 5, the fluorescence *RRMSE%* were 2.62% and 4.20% in the A and B bands, respectively. These results are shown for purposes of comparison with those obtained for the lower resolution, which are reported in Fig. 4 (second row). This case demonstrates that fluorescence can be better decoupled from reflectance terms at this resolution and sampling notwithstanding the two reflectance terms were still coupled, especially in the continuum of the B band. Furthermore, we verified that the decoupling procedure of the latter two terms in successive optimization runs did not influence the accuracy in fluorescence retrieval.

Table 2. Limiting n_l values and residuals in the A and B bands for the (AB) retrieval

ILS	*s*	*ILS/s*	n_l *(AB)*	*RMSE _A*	*RRMSE_A*	*RMSE_B*	*RRMSE_B*
cm^{-1}	cm^{-1}			W/cm^2srcm^{-1}	%	W/cm^2srcm^{-1}	%
0.380	0.200	1.90	$3.00\ 10^{-6}$	$0.22\ 10^{-8}$	1.00	$0.12\ 10^{-8}$	0.75
0.770	0.467	1.65	$1.56\ 10^{-6}$	$0.11\ 10^{-8}$	0.34	$0.64\ 10^{-9}$	0.39
	0.572	1.35	$1.26\ 10^{-6}$	$0.87\ 10^{-9}$	0.29	$0.52\ 10^{-9}$	0.31
2	1.700	1.20	10^{-6}	$0.65\ 10^{-9}$	0.17	$0.39\ 10^{-9}$	0.24

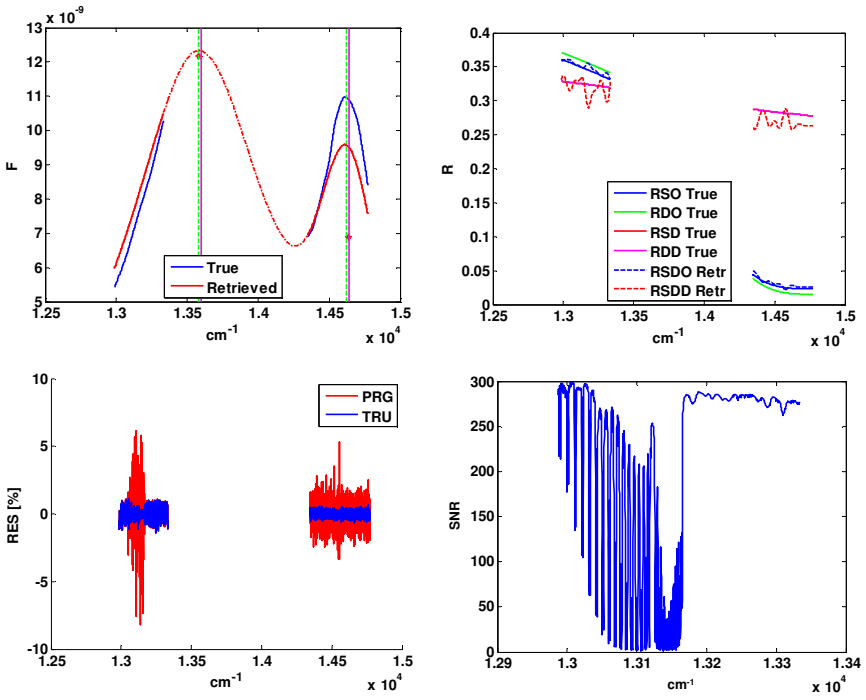

Fig. 6. Last-run retrieval of fluorescence, reflectance terms and residuals for *bare* case at a resolution of 0.38 cm^{-1}, sampling of 0.2 cm^{-1}, and noise coefficient $n_l = 3.30\ 10^{-6}$. The corresponding SNR is also reported. DS derived from a normalization to SENSOR-RAD. The peak position and intensity of each Voigt are indicated by an asterisk. The two simulated adjacency reflectance terms were equal.

However, for increasing noise, a larger number of knots was also required at the two higher resolutions, in order to obtain a certain degree of control in rather narrow spectral

#123414 - $15.00 USD Received 28 Jan 2010; revised 24 Feb 2010; accepted 2 Mar 2010; published 8 Jul 2010

ranges (about 1.5 cm^{-1}– 2 cm^{-1}). A comparison at the different resolutions was performed only in the *bare* case. In Table 2, the maximum noise coefficient n_l for an accuracy better than 10% is reported at the three resolutions in column *(AB)*. The optimization cycle consisted of about six runs for each case. At a resolution of 2 cm^{-1}, the noise coefficient corresponded to about $n_l = 10^{-6}$.

The series of runs performed with this noise is shown in Fig. 4. At the resolutions of 0.38 cm^{-1} and 0.77 cm^{-1}, we could increase the noise as reported in Table 2. This result was not surprising, since lower resolutions tend to flatten the absorption spectral features and to make less accurate the absorption line reconstruction for the evaluation of the smooth fluorescence in-filling. The sampling intervals in Table 2 corresponded to the characteristics of the sensors that worked at different resolutions. Indeed, we found that the sampling of 0.2 cm^{-1} was really important for the retrieval at TANSO-FTS resolution. The results of the two samplings suggested the importance of an effort in the direction of a higher sampling also for the OCO resolution. We found that this importance decreased at lower resolutions.

Table 3. Limiting n_l values and residuals in the (A) retrieval

ILS	*s*	*(A)*	*RRMSE* %	*RMSE* $W/cm^2\ sr\ cm^{-1}$
cm^{-1}	cm^{-1}	n_l		
0.380	0.200	$7.20\ 10^{-6}$	2.07	$0.53\ 10^{-8}$
0.770	0.467	$5.34\ 10^{-6}$	1.13	$0.37\ 10^{-8}$

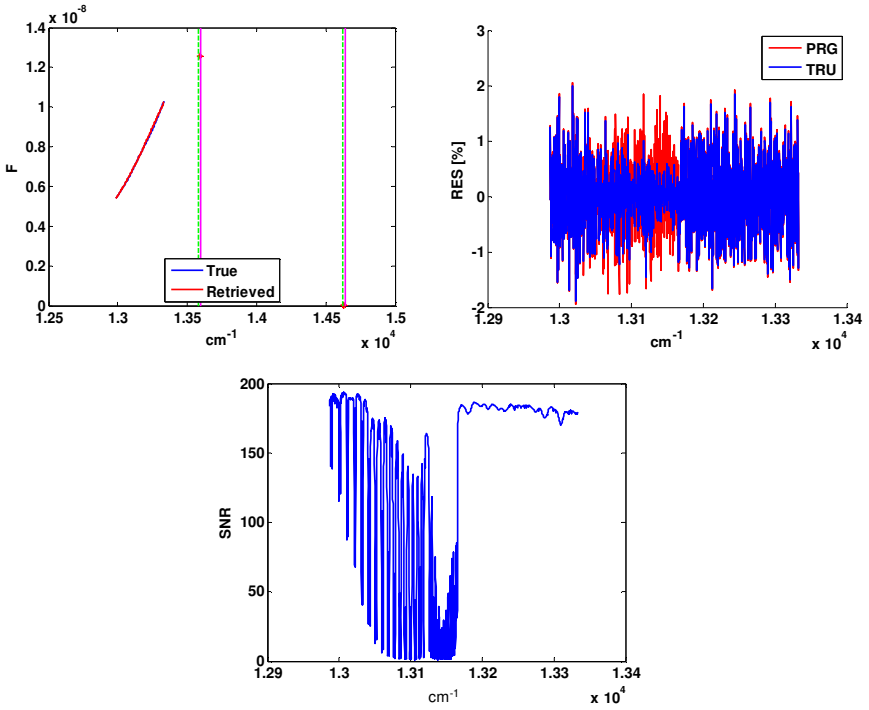

Fig. 7. Simulated and retrieved fluorescence in the A band, residuals, and SNR corresponding to an $n = 5.10\ 10^{-6}$ noise coefficient for *bare* case at a resolution of 0.38 cm^{-1}, and a sampling of 0.2 cm^{-1}. The peak position and intensity of each Voigt are indicated by an asterisk. The two simulated adjacency reflectance terms were equal. DS derived from a normalization to the square root of SENSOR_RAD.

The last run results for $n = 3.30\ 10^{-6}$ at TANSO-FTS resolution and sampling are shown in Fig. 6. We used this value because it corresponded to the minimum signal-to-noise ratio requirement of TANSO-FTS [4]. In this case, ξ differed from ρ by more than 10% (in

#123414 - $15.00 USD Received 28 Jan 2010; revised 24 Feb 2010; accepted 2 Mar 2010; published 8 Jul 2010

particular: + 13%). The corresponding fluorescence *RREMSE*% values of 7.5% and 8.3% in the A and B bands respectively, were still within an accuracy of 10%.

Retrieval solely in the A band was also performed by using only one Voigt, due to the poor influence of the second Voigt in the retrieval of fluorescence in this band. The normalization that was used in this case was to the square root of SENSOR_RAD.

In Table 3, the limiting values n_l are reported in column (A) for two resolutions. A fluorescence accuracy of better than 10% could be obtained in only one run in both cases. Fluorescence and residuals for $n = 5.10\ 10^{-6}$ are shown in Fig. 7 for the TANSO-FTS resolution. The corresponding SNR is also shown. This *n* value is smaller than the limit value for this resolution and sampling, but we have shown these results because the corresponding SNR is comparable to that of the TANSO_FTS instrument simulator [5].

Furthermore, as a useful exercise, we used the single-band retrieved amplitude of the Voigt A in order to restrict the variability range of the said Voigt in a double-band fluorescence retrieval (A-AB). By availing ourselves of this facility, we were able to increase the noise coefficient with respect to the n_l value in Table 2 for the (*AB*) case, while maintaining an accuracy of better than 10%. This (*A-AB*) case for $n = 5.10\ 10^{-6}$ is reported in Table 4, with the *RMSE* and *RRMSE* of the residuals in each band. The retrieved fluorescence is shown in Fig. 1. The accuracy in this fluorescence retrieval was 1.46% and 1.61% in the A and B bands, respectively, and was obtained with a total number of five runs. This type of retrieval will be repeated for the other two lower resolutions.

Table 4. Residuals in A and B bands for the (A-AB) retrieval

ILS	*s*	*(A-AB)*				
		n	*RMSE _A*	*RRMSE_A*	*RMSE _B*	*RRMSE_B*
cm^{-1}	cm^{-1}		W/cm^2srcm^{-1}	%	W/cm^2srcm^{-1}	%
0.380	0.200	$5.10\ 10^{-6}$	$0.36\ 10^{-8}$	1.08	$0.21\ 10^{-8}$	1.23

6. Conclusion

Fluorescence retrieval from space was demonstrated to be possible with the accuracy required by vegetation experts, thanks to the appropriate resolution of a commercial radiative transfer program (MODTRAN5 beta), a spectroscopic function for fluorescence, and cubic splines for reflectance. This was demonstrated by simulating canopy fluorescence according to a model that represented reality. We performed a fit of the results of the canopy model in order to test our algorithm and to deduce the variability ranges of the fluorescence and reflectance parameters that could be used for this type of retrieval in real conditions. The choice of the number of knots to be used for the cubic-spline reflectance fitting-functions was determined in accordance with the accuracy of the fluorescence. This method enabled us to retrieve fluorescence without imposing severe initial constraints on the reflectance terms. However, the limitations applied substantially helped to maintain the RRMSE% of fluorescence within an interesting range for space monitoring. For increasing resolution, it was found that the fluorescence was more easily decoupled from the reflectance terms, and we could therefore increase the noise, or decrease the number of runs, for the same noise. A study of the sensitivity to atmospheric (humidity, visibility, altitude) variations could then be undertaken.

Acknowledgments

M. Mazzoni wishes to thank Bruno Carli, Santina Rocchi, Alessandro Barducci, and Jose Moreno for their helpful suggestions during the development of this study. This work was partially financed by the National Research Council as a grant to M. Mazzoni. The authors wish to acknowledge ESA funding under ESTEC Contract No. 21264/07/NL/FF.

#123414 - $15.00 USD Received 28 Jan 2010; revised 24 Feb 2010; accepted 2 Mar 2010; published 8 Jul 2010